INORGANIC CHEMISTRY FRONTIERS

RESEARCH ARTICLE

View Article Online
View Journal | View Issue

Cite this: *Inorg. Chem. Front.*, 2023, **10**, 5745

Ligand-passivated Au/Cu nanoclusters with uncoordinated sites give reaction turnover numbers of up to 4 × 10^4†

Lu Dong,‡[a,b] Linke Yu,‡[c] Xueli Sun,‡[a] Xiongkai Tang,‡[d] Xuexin You,[c] Jiaqi Tang,[e] Zi-Ang Nan,[f] Dongxu Cao,[d] Yanyuan Jia,[b] Simin Li,[a] Fengyu Li, *[c] Shuo Guo *[b] and Hui Shen *[a]

Received 3rd June 2023,
Accepted 16th August 2023

DOI: 10.1039/d3qi01035j

rsc.li/frontiers-inorganic

Ligand-passivated metal nanoclusters with both high stability and catalytic activity have been pursued for a long time to shed light on the underlying rationale of ligand-functionalized metal nanocatalysts in chemical transformations. Nevertheless, these atomically precise nanocatalysts often exhibit low catalytic activity due to the extensive coverage of active sites. In this work, we report a robust gold–copper alloy nanocluster with 74 nuclei with high catalytic performance. The nanocluster with molecular composition of $Au_{41}Cu_{33}(RS)_{40}(MeCN)$ (RSH is 4-fluorothiophenol) has been obtained in a simple way. The cluster contains 34 free electrons, making it a superatom that exhibits high thermal stability as envisioned. Surprisingly, rich uncoordinated copper sites are present on the surface of the cluster, leading to its extremely high catalytic activity (up to 39 269 TON) in C–O coupling reactions with a broad substrate scope.

Introduction

Ligands have been routinely used in the synthesis of metal nanocatalysts for controlling their shape, structure, and catalytic performance.[1–4] The role of ligands when synthesizing metal nanocatalysts, however, has remained a topic of debate for a long time: although several recent studies have demonstrated their promotional effects on catalytic activity, most consider them as poisons.[4–6] It is the shortage of molecular characterization techniques for nanocatalysts that makes it more challenging to decipher how they work in the presence of extensive ligand coverage.[7–9] As a bridge between molecules and nanoparticles, atomically precise metal nanoclusters have attracted increasing interest in fundamental research in the field of catalysis due to their high degree of monodispersity, enabling the determination of their crystal structure.[10–23] In this regard, they are proposed to be model systems to rationalize the underlying reaction mechanism of metal nanocatalysts in terms of activity, selectivity, and stability.[24–28]

The past decades have witnessed an explosive increase in employing ligand-stabilized atomically precise metal nanoclusters as catalysts to drive a wide range of chemical reactions.[29–41] In catalysis, the surface ligands of metal nanoclusters are often removed by suitable thermal treatment or in some cases by automatic migration to the supports to activate the substrates.[42,43] This, however, raises another interesting doubt whether the integrity or structure of metal nanoclusters remains intact after their treatment.[44,45] To our delight, recent reports have claimed that clusters protected by bulky and rigid ligands would exhibit catalytic ability without any pre-treatment. For example, the group of Zheng demonstrated that the surface coordination of bulky N-heterocyclic carbene endowed a family of gold nanoclusters including Au_{13}, Au_{25} and Au_{44} with high catalytic activity in the activation of alkyne compounds.[46–48] Moreover, Wang and co-workers revealed that the Au_{23} cluster protected by rigid dipyridylamido and phosphine ligands exhibited high catalytic activity in the aerobic oxidation of benzyl alcohol.[49] The MAu_8 (M = Pd or Pt) series of clusters also displayed excellent catalytic hydrogenation

[a]*College of Energy Materials and Chemistry, Inner Mongolia University, Hohhot 010021, China. E-mail: shen@imu.edu.cn*
[b]*College of Chemistry and Chemical Engineering, Inner Mongolia University, Hohhot 010021, China*
[c]*School of Physical Science and Technology, Inner Mongolia University, Hohhot 010021, China*
[d]*State Key Laboratory for Physical Chemistry of Solid Surfaces, College of Chemistry and Chemical Engineering, Xiamen University, Xiamen 361005, China*
[e]*CAS Center for Excellence in Nanoscience, Beijing Key Laboratory of Micro-Nano Energy and Sensor, Beijing Institute of Nanoenergy and Nanosystems, Chinese Academy of Sciences, Beijing, 101400, China*
[f]*CAS Key Laboratory of Design and Assembly of Functional Nanostructures, and Fujian Provincial Key Laboratory of Nanomaterials, Fujian Institute of Research on the Structure of Matter, Chinese Academy of Sciences, China*

†Electronic supplementary information (ESI) available. CCDC 2211306. For ESI and crystallographic data in CIF or other electronic format see DOI: https://doi.org/10.1039/d3qi01035j

‡These authors contributed equally to this work.

ability owing to the introduction of bulky ligands, such as triphenylphosphine.[50,51] In general cases, the high activity of those clusters protected by bulky or rigid ligands relies on the presence of uncoordinated metal sites created by the repulsion between the surface ligands. Therefore, two more questions arise when employing metal nanoclusters as catalysts: 1. whether or not clusters featuring uncoordinated metal sites can be gained in the absence of bulky or rigid ligands? 2. How active can ligand-passivated metal nanoclusters be with limited numbers of exposed sites?

Herein, we report a rare example of a ligand-protected metal nanocluster with both robustness and surprisingly high catalytic activity. The new gold–copper nanocluster with 74 nuclei, with the molecular formula of $Au_{41}Cu_{33}(RS)_{40}(MeCN)$ (labeled as $Au_{41}Cu_{33}$ hereafter, RSH is 4-fluorothiophenol), has been selectively obtained by a two-step reduction strategy. The flexible thiolate ligands stabilize the metal core in a tight and diverse manner, endowing it with superatomic characteristics of 34 free electrons and high stability. What is interesting to note is that some surface-uncoordinated copper sites are available within the cluster. As a result, it exhibits an extremely high catalytic activity (up to 39 269 TON) in catalyzing Ullmann coupling reactions with a broad substrate scope without any pre-treatment.

Results and discussion

The $Au_{41}Cu_{33}$ cluster was prepared by a two-step strategy (Fig. S1, see details in the ESI†). The first step involved the $NaBH_4$-mediated reduction of $Cu(MeCN)_4BF_4$ in the presence of an appropriate amount of 4-fluorobenzenethiol, affording a brown solution (Fig. S2†). It is proposed that copper hydride species are produced in this step.[35,52] To the solution, RSAu was then added in solid form. During the aging period, the solid dissolved gradually, causing the color of the solution to change from brown to black (Fig. S2†). Layering hexane upon the black solution afforded black crystals as final products with a yield of 26.6% (based on Au, Fig. S3†). We note that the product obtained by the two-step synthetic strategy differs from that obtained by the one-step reduction of the mixture containing Cu and Au precursors, as the two strategies represent distinct reduction kinetics during the synthesis.

We first performed X-ray diffraction to determine the structure of the crystalline products (Fig. S4†). The analysis revealed that $Au_{41}Cu_{33}$ crystallizes in the triclinic system of the $Pa\bar{3}$ space group (Table S1†), with two independent clusters in each unit cell (Fig. S5†). Each cluster comprises 41 Au atoms, 33 Cu atoms, 40 thiolate ligands and one acetonitrile ligand, giving rise to a large cluster of $Au_{41}Cu_{33}(RS)_{40}(MeCN)$ ~2.4 nm in size (Fig. S6†). The absence of counterions in the lattice suggests the neutral state of the cluster.[53,54] The overall structure of $Au_{41}Cu_{33}$, shown in Fig. 1, resembles a three-necked flask in which the C_2 axis is present across the center (Fig. 1 and S7†).

The cluster adopts a core–shell architecture. As shown in Fig. 2a, the metal core of the cluster can be anatomized as a concentric Russian structure consisting of $Au@Au_{12}@Au_6@Au_{11}Cu_{33}$. The central part of the cluster core consists of an Au atom, which is surrounded by a distorted Au_{12} cage that forms a core–shell structure of Au_{13} (Fig. 2b). Interestingly, the Au_{12} cage is composed of interlaced pentagonal and triangular windows on the sides and quadrilateral ones on the top and bottom. The top window size in the Au_{12} cage (4.29 × 4.39 Å) is slightly larger than the bottom window size (4.20 × 4.37 Å). The Au_6 shell is further wrapped around the periphery of the Au_{12} cage. Of note, each Au atom of the Au_6 shell is located

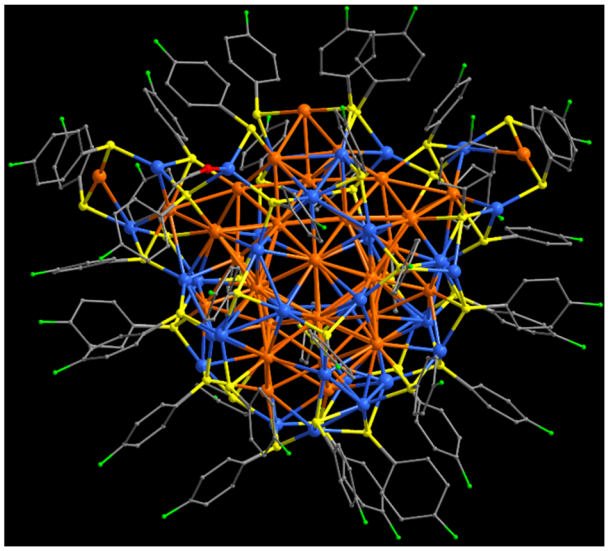

Fig. 1 Total structure of $Au_{41}Cu_{33}(RS)_{40}(MeCN)$. Color legend: orange spheres, Au; blue spheres, Cu; yellow spheres, S; turquoise spheres, F; and gray spheres, C. All hydrogen atoms are omitted for clarity.

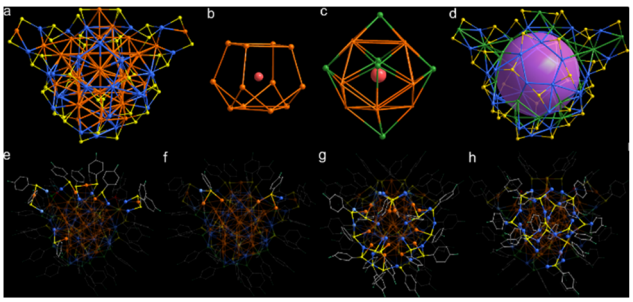

Fig. 2 Detailed structure analysis of the metal framework and coordination modes of 4-fluorothiophenol on $Au_{41}Cu_{33}(RS)_{40}(MeCN)$. (a) Layers of nested Russian nesting structures, (b) icosahedral Au_{13} core–shell structure, (c) core–shell–shell structure of the $Au@Au_{12}@Au_6$ skeleton, and (d) outermost hybrid Au–Cu–RS cage. (e) μ_2–η^1(Cu), η^1(Au) coordination mode, (f) μ_3–η^1(Cu), η^1(Au), η^1(Au) coordination mode, (g) μ_3–η^1(Cu), η^1(Cu), η^1(Au) coordination mode, and (h) μ_3–η^1(Cu), η^1(Cu), η^1(Cu) coordination mode. Color legend: orange spheres, Au; blue spheres, Cu; yellow spheres, S; turquoise spheres, F; and gray spheres, C. All hydrogen atoms are omitted for clarity. For a clearer visual representation, atoms of different shells in the diagram are shown in different colours (magenta Au in the core, orange Au in shell 1, green Au in shell 2, and blue Au and green Cu in shell 3, respectively).

outside the pentagonal and quadrilateral windows, adopting an octahedral structure for the Au_6 shell (Fig. 2c). The $Au@Au_{12}@Au_6$ skeleton is further encapsulated by a hybrid Au–Cu–RS cage that forms the Russian nesting structure of $Au_{41}Cu_{33}$ (Fig. 2d). Careful dissection of the structure reveals that, in the Au-centered icosahedral core, the average distance between the Au center and the surrounding Au_{12} shell is 3.1093 Å and in the Au_{12} shell is 2.9150 Å. These values are slightly larger than the distances in the $Au@Au_{12}$ units of other nanoclusters, *e.g.* $Au_{25}(SCH_2CH_2Ph)_{18}$, $[Au_{13}(NHC^{Bn})_9Cl_3]^{2+}$ and $[Au_{19}(PR_3)_3(C{\equiv}CR)_9]^{2+}$, indicating weak interactions.[55–57] The Au_6 octahedron caps the $Au@Au_{12}$ core tightly, as suggested by their short Au–Au bond lengths (average 2.8065 Å). The internal cavity of the Au–Cu–RS cage can be approximated as a sphere with a cavity size of about 4.6 Å, which firmly confines the gold cluster skeleton of $Au@Au_{12}@Au_6$ and thus maintains the stability of its overall structure.

The forty 4-fluorothiophenol ligands are attached to the $Au_{11}Cu_{33}$ shell to construct the complete structure of the cluster. As for the thiolate ligands on the surface, they can be divided into four types: nine thiolates are coordinated in the μ_2–η^1(Cu), η^1(Au) mode (Fig. 2e), two in μ_3–η^1(Cu), η^1(Au), η^1(Au) (Fig. 2f), sixteen in μ_3–η^1(Cu), η^1(Cu), η^1(Au) (Fig. 2g) and thirteen in μ_3–η^1(Cu), η^1(Cu), η^1(Cu) (Fig. 2h). The diverse coordination patterns of thiolates with the metal atoms of the cluster lead to its rich surface local structures: either in staple motifs or three-dimensional organometallic oligomers. The binding between the thiolates and the metal atoms is strong, as suggested by their short bond distances (2.277–2.564 Å for Au–S and 2.210–2.426 Å for Cu–S). The diverse coordination patterns of thiolates on the cluster indicate that the organic ligands not only play a key role in the stabilization of metal clusters down to the nanometer scale, but also in the creation of special local structures that facilitate related applications.

It is interesting to note that although the flexible thiolates protect the metal core of the $Au_{41}Cu_{33}$ cluster tightly, some uncoordinated copper sites are present on the surface. This can be clearly visualized by the coordination of acetonitrile molecules on the surface of the cluster. As shown in Fig. 3a, one of the surface Cu sites is covered by the ligand of acetonitrile, with a strong interaction (Cu–N bond length of 1.960 Å). On the other hand, some Cu sites are fully exposed, which may facilitate chemical transformations (see Fig. 3b).

Following the structure determination of the cluster, its electronic structure has been then studied both theoretically and experimentally. The count of free electrons of $Au_{11}Cu_{33}$ observed from its chemical formula corresponds to 34 free electrons, a number that satisfies electron shell closures. The 34 free electrons of the cluster are thus proposed to fill the "superatomic orbitals" of $1S^2|1P^6|1D^{10}|2S^2 1F^{14}|$, wherein S–P–D–F–G–H are defined as the angular momentum characters.[58] To gain insight into the electronic structure of the $Au_{41}Cu_{33}$ cluster, we further performed density functional theory (DFT) calculations using the experimental structure of the cluster as the model (see technical details in the ESI, Table S2†).[59–62] As shown in Fig. 4a and b, the $Au_{41}Cu_{33}$ cluster has a gap of 0.52 eV between the highest occupied molecular orbital (HOMO) and the lowest unoccupied molecular orbital (LUMO), and both the HOMO and the LUMO distribute on metal and S atoms. The clear HOMO–LUMO gap strongly suggests that the cluster is electronically stable as a neutral species, which is also supported by high-resolution electrospray ionization mass spectrometry and energy-dispersive X-ray spectrometry (EDS) elemental mapping (Fig. S8 and S9†). The partial density of states (PDOS) also suggests that the Au/Cu-d and S-p states dominate both frontier orbitals (see the red and orange lines in Fig. 4c). The measured ultraviolet-visible spectrum (UV-Vis) of the cluster in dichloromethane exhibits nearly no characteristic peaks (Fig. 4d). Containing 34 superatomic free electrons and rigid surface protective shells, the cluster also features high stability. As exhibited in Fig. 4e, the time-dependent UV-Vis profiles suggest that the cluster would maintain its structure in solution form upon heating at 65 °C for up to 5 hours.

Thus, with such a nanocluster of $Au_{41}Cu_{33}$, which is atomically precise, highly stable and has well-exposed metal sites, we set out to investigate in the following section its applicability

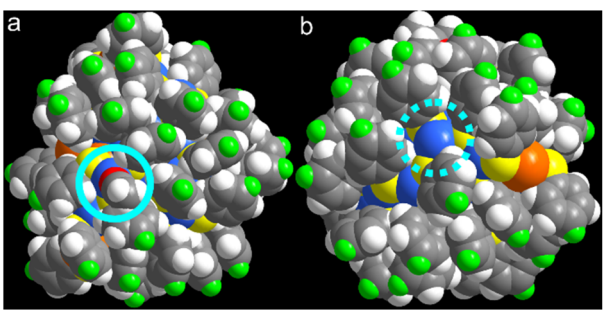

Fig. 3 $Au_{41}Cu_{33}(RS)_{40}(MeCN)$ cluster in space-filling mode showing the presence of uncoordinated atoms on the surface. Color codes for atoms: orange spheres, Au; blue spheres, Cu; magenta spheres, P; purple spheres, Sb; bright green spheres, F; and grey spheres, C. All hydrogen atoms are omitted for clarity.

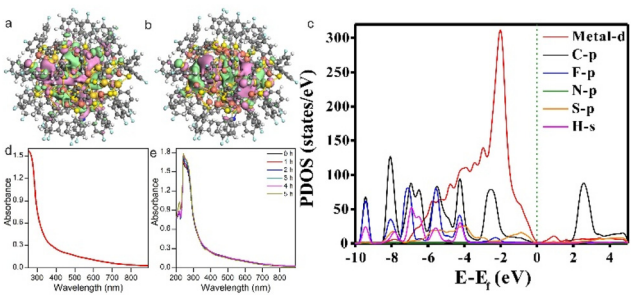

Fig. 4 (a and b) Distribution of the HOMO and the LUMO of the $Au_{41}Cu_{33}$ cluster. Color codes for atoms: Au, blue; Cu, orange; P, pink; C, gray; and H, white. (c) The projected density of states (PDOS) of the $Au_{41}Cu_{33}$ cluster. (d) UV-Vis spectra of the $Au_{41}Cu_{33}$ cluster in dichloromethane. (e) Time-dependent UV-Vis spectra of $Au_{41}Cu_{33}$ clusters dissolved in chloroform upon heating to 65 °C.

in organic synthesis (Fig. S10–19†). To our delight, this nanocluster allows preeminent catalytic performance in the C–O bond coupling reaction using aryl iodides and phenols and the results are presented in Table 1. Functional groups on the aryl rings such as trifluoromethyl (**1k** and **1r**), methoxy (**1d**, **2f**, **3g**), and nitrile (**1c**) proved to be compatible with this reaction. Furthermore, other aryl rings, such as naphthyl (**2e**) and quinolinyl (**1b**), had little influence on the reaction efficiency to give diaryl ether products in good yields. It is worth mentioning that structurally complicated substrates derived from natural products, such as eugenol and δ-tocopherol, were also well accommodated, affording the desired products (**3f** and **3h**) in moderate yields. As anticipated, the $Au_{41}Cu_{33}$ cluster, as a recyclable catalyst, presented extremely high TONs for the C–O bond coupling reaction, significantly outperforming its homogeneous counterpart, owing to its decomposition under catalytic conditions. For example, 4-phenoxybenzonitrile (**3c**) could be prepared using the catalytic system with a TON value as high as 39 269. The comparison of the TON between the $Au_{41}Cu_{33}$ cluster and several representative catalysts, including copper precursors, gold–thiolate complexes, and other gold–copper alloy nanoclusters without surface-uncoordinated metal sites, gives direct evidence of its high catalytic activity. As shown in Table S3,† the TON of the $Au_{41}Cu_{33}$ cluster is much higher than that of other reference catalysts under the same conditions, verifying its high surface reactivity.

To rationalize the high catalytic activity of the $Au_{41}Cu_{33}$ cluster and to help understand the catalytic mechanism, we performed DFT calculations to probe the reactive sites. The DFT calculations (see Table S4 and Fig. S20†) reveal that the adjacent uncoordinated copper sites have a stronger interaction with C_6H_5–I and C_6H_5–OH than the other copper sites do by about 0.2 and 0.5 eV, respectively. This suggests that the uncoordinated copper sites facilitate the formation of HI and C_6H_5–O–C_6H_5. The $Au_{41}Cu_{33}$ catalyst exhibits not only high catalytic activity, but also high stability. As shown in Fig. S21,† the catalytic activity of $Au_{41}Cu_{33}$/XC-72 remains nearly unchanged after three cycles. The identical UV-Vis profiles of $Au_{41}Cu_{33}/TiO_2$ before and after catalysis further suggest its high stability during the catalysis (Fig. S22†). These results indicate that the $Au_{41}Cu_{33}$ catalyst is practically useful to prepare a variety of diaryl ether compounds.

Table 1 $Au_{41}Cu_{33}$-catalyzed C–O bond coupling reaction with high TONs[a]

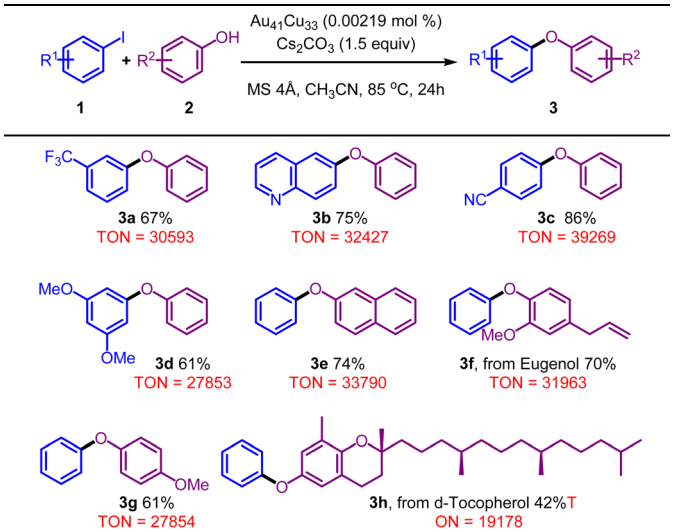

[a] Standard conditions: $Au_{41}Cu_{33}$ (0.00219 mol%), **1** (1.8 mmol, 1.2 equiv.), **2** (1.2 mmol, 1 equiv.), MS 4 Å (20 mg), in CH_3CN (1.2 mL), stirred at 85 °C for 24 h. Yield of isolated products.

Conclusion

In conclusion, a new atomically precise Au/Cu nanocluster with 74 nuclei stabilized by flexible thiolates has been obtained. Owing to both electronic and steric closures, the cluster exhibits moderate stability. The most important feature of the cluster relies on the presence of uncoordinated metal sites on its surface, making it a good candidate for catalyzing Ullmann reactions with high activity and a broad reactant scope. This work demonstrates that the stability and catalytic activity of ligand-stabilized metal nanoclusters can be well balanced by delicately tailoring the local structure of the surface. Also, it provides, at the molecular level, the rationale for the catalytic performance of ligand-functionalized metal nanocatalysts.

Author contributions

Hui Shen supervised the project. Lu Dong carried out most of the characterization and catalysis under the guidance of Hui Shen and Shuo Guo. Xueli Sun and Xiongkai Tang prepared the cluster samples and conducted part of the characterization studies. Jiaqi Tang, Zi-Ang Nan, Dongxu Cao, Yanyuan Jia and Simin Li conducted part of the characterization studies. Linke Yu and Xuexin You conducted DFT calculations under the guidance of Fengyu Li. All authors were responsible for analyzing the data and composing the manuscript. Lu Dong, Linke Yu, Xueli Sun, and Xiongkai Tang contributed equally to this work.

Conflicts of interest

There are no conflicts to declare.

Acknowledgements

H. S. expresses his greatest appreciation to Professor Nanfeng Zheng (Xiamen University) for his generous support. H. S. acknowledges the financial support from the Program for Young Talents of Science and Technology in the Universities of Inner Mongolia Autonomous Region (NJYT23035) and the start-up funding of Inner Mongolia University (10000-

23112101/043). F. L. expresses gratitude for the financial support from the National Natural Science Foundation of China (11964024), the "Grassland Talents" project of the Inner Mongolia Autonomous Region (12000-12102613) and the Young Science and Technology Talents Cultivation Project of Inner Mongolia University (21200-5223708). S. G. acknowledges the financial support by the Program for Young Talents of Science and Technology in the Universities of Inner Mongolia Autonomous Region (NJYT22091), the Natural Science Foundation of Inner Mongolia Autonomous Region of China (2021BS02002), and the Young Science and Technology Talents Cultivation Project of Inner Mongolia University (No. 21221505). Y. J. acknowledges the financial support from the Natural Science Foundation of Inner Mongolia Autonomous Region of China (2022QN02015) and the Research Program of Science and Technology at the Universities of Inner Mongolia Autonomous Region (NJZY22334).

References

1 C. Xie, Z. Niu, D. Kim, M. Li and P. Yang, Surface and Interface Control in Nanoparticle Catalysis, *Chem. Rev.*, 2020, **120**, 1184–1249.
2 K. Liu, R. Qin and N. F. Zheng, Insights into the Interfacial Effects in Heterogeneous Metal Nanocatalysts toward Selective Hydrogenation, *J. Am. Chem. Soc.*, 2021, **143**, 4483–4499.
3 A. Verma, O. Uzun, Y. Hu, Y. Hu, H. Han, N. Watson, S. Chen, D. J. Irvine and F. Stellacci, Surface-structure-regulated cell-membrane penetration by monolayer-protected nanoparticles, *Nat. Mater.*, 2008, **7**, 588–595.
4 T. Xue, Z. Lin, C. Chiu, Y. Li, L. Ruan, G. Wang, Z. Zhao, C. Lee, X. Duan and Y. Huang, Molecular ligand modulation of palladium nanocatalysts for highly efficient and robust heterogeneous oxidation of cyclohexenone to phenol, *Sci. Adv.*, 2017, **3**, e1600615.
5 A. Heuer-Jungemann, N. Feliu, I. Bakaimi, M. Hamaly, A. Alkilany, I. Chakraborty, A. Masood, M. F. Casula, A. Kostopoulou, E. Oh, K. Susumu, M. H. Stewart, I. L. Medintz, E. Stratakis, W. J. Parak and A. G. Kanaras, The Role of Ligands in the Chemical Synthesis and Applications of Inorganic Nanoparticles, *Chem. Rev.*, 2019, **119**, 4819–4880.
6 T. Kawawaki, Y. Kataoka, M. Hirata, Y. Iwamatsu, S. Hossain and Y. Negishi, Toward the creation of high-performance heterogeneous catalysts by controlled ligand desorption from atomically precise metal nanoclusters, *Nanoscale Horiz.*, 2021, **6**, 409–448.
7 H. Häkkinen, The gold–sulfur interface at the nanoscale, *Nat. Chem.*, 2012, **4**, 443–455.
8 X. Liu, M. Yu, H. Kim, M. Mameli and F. Stellacci, Determination of monolayer-protected gold nanoparticle ligand–shell morphology using NMR, *Nat. Commun.*, 2012, **3**, 1182.
9 Z. Wang, L. A. Völker, T. C. Robinson, N. Kaeffer, G. Menzildjian, R. Jabbour, A. Venkatesh, D. Gajan, A. J. Rossini, C. Copéret and A. Lesage, Speciation and Structures in Pt Surface Sites Stabilized by N-Heterocyclic Carbene Ligands Revealed by Dynamic Nuclear Polarization Enhanced Indirectly Detected ^{195}Pt NMR Spectroscopic Signatures and Fingerprint Analysis, *J. Am. Chem. Soc.*, 2022, **144**, 21530–21543.
10 C. Sun, B. K. Teo, C. Deng, J. Lin, G. Luo, C. H. Tung and D. Sun, Hydrido-coinage-metal clusters: Rational design, synthetic protocols and structural characteristics, *Coord. Chem. Rev.*, 2021, **427**, 213576.
11 H. Shen, G. Tian, Z. Xu, L. Wang, Q. Wu, Y. Zhang, B. K. Teo and N. F. Zheng, N-heterocyclic carbene coordinated metal nanoparticles and nanoclusters, *Coord. Chem. Rev.*, 2022, **458**, 214425.
12 R. Jin, C. Zeng, M. Zhou and Y. Chen, Atomically Precise Colloidal Metal Nanoclusters and Nanoparticles: Fundamentals and Opportunities, *Chem. Rev.*, 2016, **116**, 10346–10413.
13 Q. Yao, T. Chen, X. Yuan and J. Xie, Toward Total Synthesis of Thiolate-Protected Metal Nanoclusters, *Acc. Chem. Res.*, 2018, **51**, 1338–1348.
14 Z. Lei, X. K. Wan, S. F. Yuan, Z. J. Guan and Q. M. Wang, Alkynyl Approach toward the Protection of Metal Nanoclusters, *Acc. Chem. Res.*, 2018, **51**, 2465–2474.
15 K. Konishi, M. Iwasaki and Y. Shichibu, Phosphine-Ligated Gold Clusters with Core + exo Geometries: Unique Properties and Interactions at the Ligand-Cluster Interface, *Acc. Chem. Res.*, 2018, **51**, 3125–3133.
16 A. Ghosh, O. F. Mohammed and O. M. Bakr, Atomic-Level Doping of Metal Clusters, *Acc. Chem. Res.*, 2018, **51**, 3094–3103.
17 Z. Gan, N. Xia and Z. Wu, Discovery, Mechanism, and Application of Antigalvanic Reaction, *Acc. Chem. Res.*, 2018, **51**, 2774–2783.
18 P. Maity, S. Takano, S. Yamazoe, T. Wakabayashi and T. Tsukuda, Binding Motif of Terminal Alkynes on Gold Clusters, *J. Am. Chem. Soc.*, 2013, **135**, 9450–9457.
19 S. Takano and T. Tsukuda, Chemically Modified Gold/Silver Superatoms as Artificial Elements at Nanoscale: Design Principles and Synthesis Challenges, *J. Am. Chem. Soc.*, 2021, **143**, 1683–1698.
20 T. Chiu, J. Liao, F. Gam, Y. Wu, X. Wang, S. Kahlal, J. Saillard and C. W. Liu, Hydride-Containing Eight-Electron Pt/Ag Superatoms: Structure, Bonding, and Multi-NMR Studies, *J. Am. Chem. Soc.*, 2022, **144**, 10599–10607.
21 J. Huang, Y. Si, X. Dong, Z. Wang, L. Liu, S. Q. Zang and T. C. W. Mak, Symmetry Breaking of Atomically Precise Fullerene-like Metal Nanoclusters, *J. Am. Chem. Soc.*, 2021, **143**, 12439–12444.
22 J. Wang, Z. Wang, S. Li, S. Q. Zang and T. C. W. Mak, Carboranealkynyl-Protected Gold Nanoclusters: Size Conversion and UV/Vis–NIR Optical Properties, *Angew. Chem., Int. Ed.*, 2021, **60**, 5959–5964.

23 H. Xu, N. V. Tkachenko, Z. Wang, W. Chen, L. Qiao, A. Muñoz-Castro, A. I. Boldyrev and Z. Sun, A sandwich-type cluster containing Ge@Pd_3 planar fragment flanked by aromatic nonagermanide caps, *Nat. Commun.*, 2020, **11**, 5286.

24 Y. Du, H. Sheng, D. Astruc and M. Zhu, Atomically Precise Noble Metal Nanoclusters as Efficient Catalysts: A Bridge between Structure and Properties, *Chem. Rev.*, 2020, **120**, 526–622.

25 E. C. Tyo and S. Vajda, Catalysis by clusters with precise numbers of atoms, *Nat. Nanotechnol.*, 2015, **10**, 577–588.

26 S. Mitchell, R. Qin, N. F. Zheng and J. Pérez-Ramírez, Nanoscale engineering of catalytic materials for sustainable technologies, *Nat. Nanotechnol.*, 2021, **16**, 129–139.

27 J. Yan, B. K. Teo and N. F. Zheng, Surface Chemistry of Atomically Precise Coinage-Metal Nanoclusters: From Structural Control to Surface Reactivity and Catalysis, *Acc. Chem. Res.*, 2018, **51**, 3084–3093.

28 F. Sun, Q. Tang and D. Jiang, Theoretical Advances in Understanding and Designing the Active Sites for Hydrogen Evolution Reaction, *ACS Catal.*, 2022, **12**, 8404–8433.

29 M. R. Narouz, K. M. Osten, P. J. Unsworth, R. W. Y. Man, K. Salorinne, S. Takano, R. Tomihara, S. Kaappa, S. Malola, C. T. Dinh, J. D. Padmos, K. Ayoo, P. J. Garrett, M. Nambo, J. H. Horton, E. H. Sargent, H. Häkkinen, T. Tsukuda and C. M. Crudden, N-heterocyclic carbene-functionalized magic-number gold nanoclusters, *Nat. Chem.*, 2019, **11**, 419–425.

30 H. Shen, Q. Wu, M. Asre Hazer, X. Tang, Y. Han, R. Qin, C. Ma, S. Malola, B. K. Teo, H. Häkkinen and N. F. Zheng, Regioselective hydrogenation of alkenes over atomically dispersed Pd sites on NHC-stabilized bimetallic nanoclusters, *Chem*, 2022, **8**, 2380–2392.

31 Y. Zhu, H. Qian, B. Drake and R. Jin, Atomically Precise $Au_{25}(SR)_{18}$ Nanoparticles as Catalysts for the Selective Hydrogenation of α,β-Unsaturated Ketones and Aldehydes, *Angew. Chem., Int. Ed.*, 2010, **49**, 1295–1298.

32 M. Zhao, S. Huang, Q. Fu, W. Li, R. Guo, Q. Yao, F. Wang, P. Cui, C. H. Tung and D. Sun, Ambient Chemical Fixation of CO_2 Using a Robust Ag_{27} Cluster-Based Two-Dimensional Metal-Organic Framework, *Angew. Chem., Int. Ed.*, 2020, **59**, 20031–20036.

33 K. Yonesato, S. Yamazoe, D. Yokogawa, K. Yamaguchi and K. Suzuki, A Molecular Hybrid of an Atomically Precise Silver Nanocluster and Polyoxometalates for H_2 Cleavage into Protons and Electrons, *Angew. Chem., Int. Ed.*, 2021, **60**, 16994–16998.

34 D. Yang, W. Pei, S. Zhou, J. Zhao, W. Ding and Y. Zhu, Controllable Conversion of CO_2 on Non-Metallic Gold Clusters, *Angew. Chem., Int. Ed.*, 2020, **59**, 1919–1924.

35 C. Sun, N. Mammen, S. Kaappa, P. Yuan, G. Deng, C. Zhao, J. Yan, S. Malola, K. Honkala, H. Häkkinen, B. K. Teo and N. F. Zheng, Atomically Precise, Thiolated Copper–Hydride Nanoclusters as Single-Site Hydrogenation Catalysts for Ketones in Mild Conditions, *ACS Nano*, 2019, **13**, 5975–5986.

36 F. Fu, J. Xiang, H. Cheng, L. Cheng, H. Chong, S. Wang, P. Li, S. Wei, M. Zhu and Y. Li, A Robust and Efficient Pd_3 Cluster Catalyst for the Suzuki Reaction and Its Odd Mechanism, *ACS Catal.*, 2017, **7**, 1860–1867.

37 Y. Zhao, S. Zhuang, L. Liao, C. Wang, N. Xia, Z. Gan, W. Gu, J. Li, H. Deng and Z. Wu, A Dual Purpose Strategy to Endow Gold Nanoclusters with Both Catalysis Activity and Water Solubility, *J. Am. Chem. Soc.*, 2020, **142**, 973–977.

38 A. Sagadevan, A. Ghosh, P. Maity, O. F. Mohammed, O. M. Bakr and M. Rueping, Visible-Light Copper Nanocluster Catalysis for the C–N Coupling of Aryl Chlorides at Room Temperature, *J. Am. Chem. Soc.*, 2022, **144**, 12052–12061.

39 J. Dong, J. R. Robinson, Z. Gao and L. Wang, Selective Semihydrogenation of Polarized Alkynes by a Gold Hydride Nanocluster, *J. Am. Chem. Soc.*, 2022, **144**, 12501–12509.

40 Z. Gao, K. Wei, T. Wu, J. Dong, D. Jiang, S. Sun and L. Wang, A Heteroleptic Gold Hydride Nanocluster for Efficient and Selective Electrocatalytic Reduction of CO_2 to CO, *J. Am. Chem. Soc.*, 2022, **144**, 5258–5262.

41 Z. Qin, S. Sharma, C. Wan, S. Malola, W. Xu, H. Häkkinen and G. Li, A Homoleptic Alkynyl-Ligated $[Au_{13}Ag_{16}L_{24}]_3^-$ Cluster as a Catalytically Active Eight-Electron Superatom, *Angew. Chem., Int. Ed.*, 2021, **60**, 970–975.

42 O. Lopez-Acevedo, K. A. Kacprzak, J. Akola and H. Häkkinen, Quantum size effects in ambient CO oxidation catalysed by ligand-protected gold clusters, *Nat. Chem.*, 2010, **2**, 329–334.

43 B. Zhang, A. Sels, G. Salassa, S. Pollitt, V. Truttmann, C. Rameshan, J. Llorca, W. Olszewski, G. Rupprechter, T. Bürgi and N. Barrabés, Ligand Migration from Cluster to Support: A Crucial Factor for Catalysis by Thiolate-protected Gold Clusters, *ChemCatChem*, 2018, **10**, 5372–5376.

44 A. W. Cook, Z. R. Jones, G. Wu, S. L. Scott and T. W. Hayton, An Organometallic Cu_{20} Nanocluster: Synthesis, Characterization, Immobilization on Silica, and "Click" Chemistry, *J. Am. Chem. Soc.*, 2018, **140**, 394–400.

45 W. Jing, H. Shen, R. Qin, Q. Wu, K. Liu and N. F. Zheng, Surface and Interface Coordination Chemistry Learned from Model Heterogeneous Metal Nanocatalysts: From Atomically Dispersed Catalysts to Atomically Precise Clusters, *Chem. Rev.*, 2022, **123**, 5948–6002.

46 H. Shen, S. Xiang, Z. Xu, C. Liu, X. Li, C. Sun, S. Lin, B. K. Teo and N. F. Zheng, Superatomic Au_{13} clusters ligated by different N-heterocyclic carbenes and their ligand-dependent catalysis, photoluminescence, and proton sensitivity, *Nano Res.*, 2020, **13**, 1908–1911.

47 H. Shen, Z. Xu, M. S. A. Hazer, Q. Wu, J. Peng, R. Qin, S. Malola, B. K. Teo, H. Häkkinen and N. F. Zheng, Surface Coordination of Multiple Ligands Endows N-Heterocyclic Carbene-Stabilized Gold Nanoclusters with High Robustness and Surface Reactivity, *Angew. Chem., Int. Ed.*, 2021, **60**, 3752–3758.

48 H. Shen, G. Deng, S. Kaappa, T. Tan, Y. Z. Han, S. Malola, S. C. Lin, B. K. Teo, H. Häkkinen and N. F. Zheng, Highly Robust but Surface-Active: An N-Heterocyclic Carbene-

Stabilized Au_{25} Nanocluster, *Angew. Chem., Int. Ed.*, 2019, **58**, 17731–17735.

49 S. F. Yuan, Z. Lei, Z. Guan and Q. M. Wang, Atomically Precise Preorganization of Open Metal Sites on Gold Nanoclusters with High Catalytic Performance, *Angew. Chem., Int. Ed.*, 2021, **60**, 5225–5229.

50 M. A. Aubart, B. D. Chandler, R. A. T. Gould, D. A. Krogstad, M. F. J. Schoondergang and L. H. Pignolet, Dihydrogen Activation by Mixed Platinum- and Palladium-Gold Cluster Compounds. Homogeneous Catalytic H_2-D_2 Equilibration, *Inorg. Chem.*, 1994, **33**, 3724–3734.

51 M. A. Aubart and L. H. Pignolet, The catalysis of hydrogen-deuterium equilibration by platinum-gold cluster compounds, *J. Am. Chem. Soc.*, 1992, **114**, 7901–7903.

52 Q. Tang, Y. Lee, D. Y. Li, W. Choi, C. W. Liu, D. Lee and D. Jiang, Lattice-Hydride Mechanism in Electrocatalytic CO_2 Reduction by Structurally Precise Copper-Hydride Nanoclusters, *J. Am. Chem. Soc.*, 2017, **139**, 9728–9736.

53 B. Han, Z. Liu, L. Feng, Z. Wang, R. K. Gupta, C. M. Aikens, C. Tung and D. Sun, Polymorphism in Atomically Precise Cu_{23} Nanocluster Incorporating Tetrahedral $[Cu_4]_0$ Kernel, *J. Am. Chem. Soc.*, 2020, **142**, 5834–5841.

54 E. F. Wilson, H. Abbas, B. J. Duncombe, C. Streb, D. Long and L. Cronin, Probing the Self-Assembly of Inorganic Cluster Architectures in Solution with Cryospray Mass Spectrometry: Growth of Polyoxomolybdate Clusters and Polymers Mediated by Silver(I) Ions, *J. Am. Chem. Soc.*, 2008, **130**, 13876–13884.

55 X. Wan, Q. Tang, S. F. Yuan, D. Jiang and Q. M. Wang, Au_{19} Nanocluster Featuring a V-Shaped Alkynyl–Gold Motif, *J. Am. Chem. Soc.*, 2015, **137**, 652–655.

56 M. Zhu, C. M. Aikens, F. J. Hollander, G. C. Schatz and R. Jin, Correlating the Crystal Structure of A Thiol-Protected Au_{25} Cluster and Optical Properties, *J. Am. Chem. Soc.*, 2008, **130**, 5883–5885.

57 M. R. Narouz, S. Takano, P. A. Lummis, T. I. Levchenko, A. Nazemi, S. Kaappa, S. Malola, G. Yousefalizadeh, L. A. Calhoun, K. G. Stamplecoskie, H. Häkkinen, T. Tsukuda and C. M. Crudden, Robust, Highly Luminescent Au_{13} Superatoms Protected by N-Heterocyclic Carbenes, *J. Am. Chem. Soc.*, 2019, **141**, 14997–15002.

58 M. Walter, J. Akola, O. Lopez-Acevedo, P. D. Jadzinsky, G. Calero, C. J. Ackerson, R. L. Whetten, H. Grönbeck and H. Häkkinen, A unified view of ligand-protected gold clusters as superatom complexes, *Proc. Natl. Acad. Sci. U. S. A.*, 2008, **105**, 9157–9162.

59 J. P. Perdew, K. Burke and M. Ernzerhof, Generalized Gradient Approximation Made Simple, *Phys. Rev. Lett.*, 1996, **77**, 3865.

60 B. Delley, An all-electron numerical method for solving the local density functional for polyatomic molecules, *J. Chem. Phys.*, 1990, **92**, 508–517.

61 B. Delley, From molecules to solids with the $DMol^3$ approach, *J. Chem. Phys.*, 2000, **113**, 7756–7764.

62 R. S. Mulliken, Electronic Population Analysis on LCAO–MO Molecular Wave Functions. I, *J. Chem. Phys.*, 1955, **23**, 1833–1840.